

# CeFePO: $f$ - $d$ hybridization and quenching of superconductivity

M.G. Holder,<sup>1</sup> A. Jesche,<sup>2</sup> P. Lombardo,<sup>3</sup> R. Hayn,<sup>3</sup> D. V. Vyalikh,<sup>1</sup> S. Danzenbächer,<sup>1</sup> K. Kummer,<sup>1</sup> C. Krellner,<sup>2</sup> C. Geibel,<sup>2</sup> Yu. Kucherenko,<sup>4</sup> T. Kim,<sup>5</sup> R. Follath,<sup>6</sup> S. L. Molodtsov,<sup>1</sup> and C. Laubschat<sup>1</sup>

<sup>1</sup>*Institut für Festkörperphysik, Technische Universität Dresden, D-01062 Dresden, Germany*

<sup>2</sup>*Max-Planck-Institut für Chemische Physik fester Stoffe, D-01187 Dresden, Germany*

<sup>3</sup>*Laboratoire Matériaux et Microélectronique de Provence associé au Centre National de la Recherche Scientifique, 13397 Marseille, France*

<sup>4</sup>*Institute for Metal Physics, National Academy of Sciences of Ukraine, UA-03142 Kiev, Ukraine*

<sup>5</sup>*Institut für Festkörperforschung, IFW Dresden, D-01171 Dresden, Germany*

<sup>6</sup>*Helmholtz-Zentrum Berlin für Materialien und Energie GmbH, Elektronenspeicherring BESSY II, D-12489 Berlin, Germany*

(Dated: April 28, 2021)

Being homologue to the new, Fe-based type of high-temperature superconductors, CeFePO exhibits magnetism, Kondo and heavy-fermion phenomena. We experimentally studied the electronic structure of CeFePO by means of angle-resolved photoemission spectroscopy. In particular, contributions of the Ce  $4f$ -derived states and their hybridization to the Fe  $3d$  bands were explored using both symmetry selection rules for excitation and their photoionization cross-section variations as a function of photon energy. It was experimentally found – and later on confirmed by LDA as well as DMFT calculations – that the Ce  $4f$  states hybridize to the Fe  $3d$  states of  $d_{3z^2-r^2}$  symmetry near the Fermi level that discloses their participation in the occurring electron-correlation phenomena and provides insight into mechanism of superconductivity in oxopnictides.

PACS numbers: 71.27.+a, 79.60.-i, 74.25.Jb

The unusual superconducting properties of the novel Fe-based oxopnictides with transition temperatures ( $T_c$ ) up to 55 K have attracted considerable attention [1–4]. While pure  $R\text{FeAsO}$  ( $R$ : rare-earth elements) compounds reveal metallic properties, doping by F on O sites leads to superconductivity. The proximity of the superconducting state to spin-density wave formation gave rise to speculations that the underlying pairing mechanism is based on magnetic fluctuations [5]. Superconductivity without doping, although at reduced  $T_c$  with respect to the arsenides, is found in the isoelectronic phosphides, except for  $R=\text{Ce}$  [6, 7]. In CeFeAsO both Fe and Ce order antiferromagnetically below a Neel temperature of 140 K [8] and 3.7 K [9], respectively. A gradual replacement of As by P leads first to the vanishing of the Fe magnetism, coupled with a change of the Ce order to ferromagnetism [10]. For further P doping the Ce order is suppressed, resulting in a paramagnetic heavy-fermion compound [11].

This wide variation of properties is a consequence of a strong sensitivity of the valence-band (VB) structure to the lattice parameters and to interaction with localized  $f$  states. Close to the Fermi level ( $E_F$ ) the electronic structure of  $R\text{FePnO}$  ( $Pn$ : phosphorus or arsenic) materials is dominated by five energy bands that have predominantly Fe  $3d$  character [12, 13]. Small variations of the lattice parameters affect particularly two of these bands, namely those containing  $d_{xy}$  and  $d_{3z^2-r^2}$  orbitals. Increasing the distance of the pnictogen ions to the Fe plane shifts the  $d_{xy}$ -derived band towards lower and the  $d_{3z^2-r^2}$ -derived bands towards higher binding energies (BE) leading to a transition from 3D to 2D behavior of the Fermi surface (FS). As discussed in Ref. [13], superconductivity delicately depends on nesting conditions between the FS sheets generated by the above mentioned bands around the  $\Gamma$  point and those located around the  $M$  point in the Brillouin zone (BZ). The nesting conditions may be affected by varia-

tions of the lattice parameters or interaction with  $4f$  states.

Purpose of the present work is to study the electronic structure of CeFePO by means of angle-resolved photoemission (ARPES) in order to understand possible reasons for the quenching of superconductivity. We find that closely below  $E_F$  both the position and the dispersion of the valence bands are strongly changed with respect to the ones in LaFePO what is at least partly due to interactions with the Ce  $4f$  states. Hybridization of the Fe  $3d$ -derived VBs and the Ce  $4f$  states leads around the  $\bar{\Gamma}$  point of the surface BZ to strong  $4f$  admixture to the valence bands, accompanied by a reconstruction of the Fermi surface and a shift of the  $4f$ -derived quasiparticle band to lower binding energies.

Experiments were performed at the “ $1^3$ -ARPES” setup at BESSY (Berlin) as described in Ref. [14], at temperatures around 10 K, on single crystals grown from a Sn flux as specified in Ref. [15]. Due to setup geometry, the vector potential  $\mathbf{A}$  of incident light is parallel to sample surface at vertical polarization (VP) and posses an additional perpendicular component at horizontal polarization (HP). Dipole matrix elements for the photoexcitation depend on the spatial extension of the orbital along the direction of  $\mathbf{A}$ . This means that in normal emission geometry states of  $d_{3z^2-r^2}$  symmetry will contribute only at HP, while those of  $d_{xz,yz}$  and  $d_{x^2-y^2}$  ( $d_{xy}$ , depending on the orientation of the sample in the  $(x, y)$  plane) symmetry will be detected at both VP and HP – though with different relative intensities.

Photoemission (PE) spectra of Ce systems reveal a well known double-peak structure consisting of a component at about 2 eV BE, roughly reflecting the  $4f^0$  final state expected from PE excitation of an unhybridized  $4f^1$  ground state, and a feature close to  $E_F$  that is only due to hybridization and reproduces the ground-state configuration of mainly  $4f^1$  character. In our measurements we made use of strong varia-

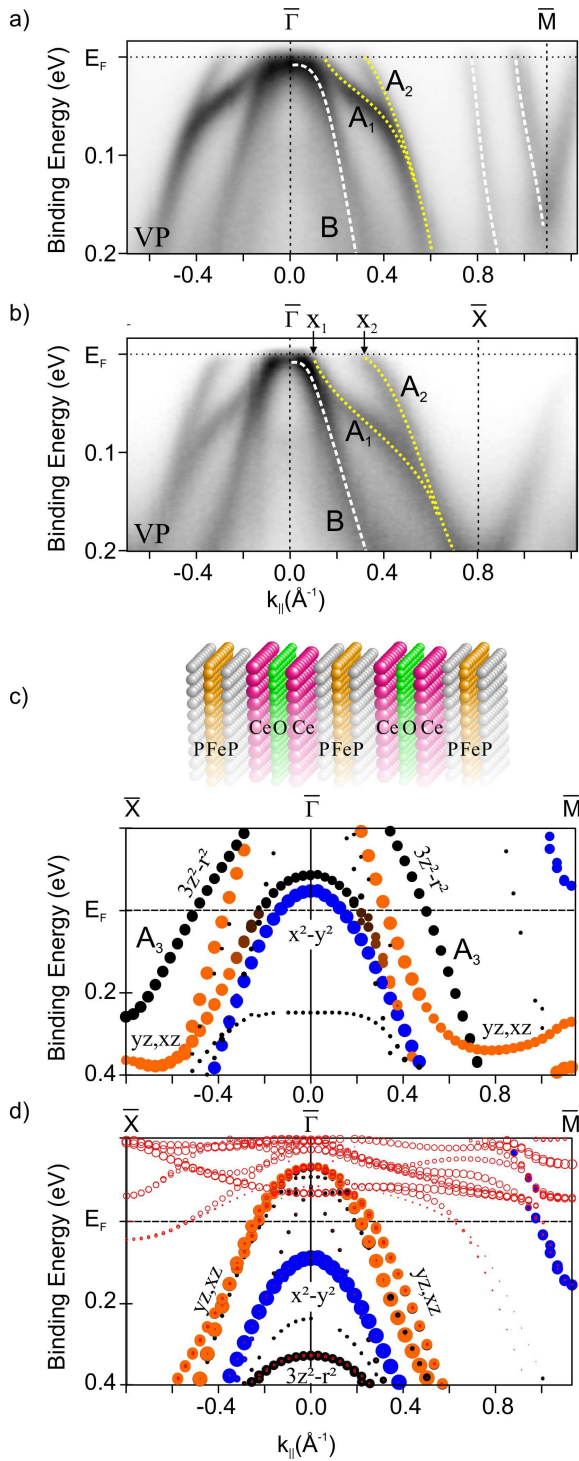


FIG. 1: (Color online) Experimental ARPES images recorded from CeFePO at  $h\nu=112$  eV and VP along the  $\bar{\Gamma} - \bar{M}$  (a) and  $\bar{\Gamma} - \bar{X}$  (b) directions in the surface BZ, and calculated energy bands for a slab containing 15 atomic layers, with a P terminated surface, treating  $4f$  states as quasi-core (c) and valence states (d). Size of the dots indicates contribution of  $d$  orbitals of the outermost Fe layer (solid dots) or of Ce  $4f$  states (4th layer, open dots). The labels indicate the orbitals with strongest contribution to the bands.

tions of the  $4f$  photoionization cross section around the  $4d \rightarrow 4f$  absorption threshold due to a Fano resonance:  $4f$  emission becomes resonantly enhanced (suppressed) at  $h\nu=121$  eV (112 eV) photon energy [16].

Valence-band maps taken at VP and a photon energy of 112 eV are shown in Fig. 1(a) and (b) for two high symmetry directions in the surface Brillouin zone. Along the  $\bar{\Gamma} - \bar{X}$  direction two energy bands cross  $E_F$  at  $x_1 \approx 0.1 \bar{\Gamma}\bar{X}$  ( $A_1$ ) and  $x_2 \approx 0.4 \bar{\Gamma}\bar{X}$  ( $A_2$ ), respectively. In LaFePO similar bands are observed but the crossings occur closer to the  $\bar{X}$  point at  $x_1 \approx 0.2 \bar{\Gamma}\bar{X}$  and  $x_2 \approx 0.7 \bar{\Gamma}\bar{X}$  [17]. In the vicinity of the  $\bar{M}$  point two additional bands can be distinguished [Fig. 1(a), dashed], that merge in LaFePO. All these bands are discussed in Ref. [17] on the basis of LDA bulk band-structure calculations, using internally relaxed parameters and rescaling calculated band energies by a factor of two. In this way, the Fermi level crossings  $x_1$  and  $x_2$  are caused by  $d_{xz,yz}$  and  $d_{3z^2-r^2}$ -derived states, respectively. The latter should hardly be visible at VP and hence at least for the present measurement a different character of the  $A_2$  band has to be concluded. Another parabolic hole-like band (labeled  $B$ ) comes very close to  $E_F$  and has no direct counterpart in LaFePO.

In order to take account of the surface sensitivity of ARPES and the fact that band positions of surface and subsurface atomic layers may be different in BE with respect to the bulk ones [18], slab calculations were performed by means of the linear-muffin-tin-orbital (LMTO) method [19]. It follows from the structural and cohesive properties that the Ce-FePO crystal can be cleaved mainly between the FeP and CeO stacks, so that the surface will be terminated either by P or Ce atoms. In the case of a P terminated slab the Fe atoms occupy the second (subsurface) layer and the main contribution to the PE intensity stems from the high cross section Fe  $3d$ -derived bands. A schematic view of the 15 atomic layer thick slab as well as results of the respective slab calculations are shown in Fig. 1(c). Note that  $4f$  states were treated as quasi-core states in order to avoid the well known failures of LDA in describing strongly localized states. The effect of the surface to the observed bands can be explained to some extent with the spatial orientation of the involved Fe  $d$  states. The calculated band structure of Fe layer in the center of the slab is very close to the bulk band structure.

Band  $B$  is quite well described by  $d_{x^2-y^2}$  states which are not strongly influenced by surface effects, since these orbitals are oriented in the  $(x,y)$  plane and contribute to the Fe-P bonds but with negligible overlap with Ce states. Two bands of  $d_{xz}$  and  $d_{yz}$  symmetry cross the Fermi level in the same way as bands  $A_1$  and  $A_2$ . Close to the  $\bar{\Gamma}$  point band  $A_1$  reveals increasing  $d_{3z^2-r^2}$  character. Besides these bands the calculation predicts a further band ( $A_3$ ) of  $d_{3z^2-r^2}$  character closer to the  $\bar{X}$  point, resembling the situation reported in LaFePO [17]. However, this band does not appear in the above ARPES maps, because this emission is symmetry forbidden in the case of VP excitation. Our calculations show that the  $d_{3z^2-r^2}$  states (and to a minor degree bands of  $d_{xz}$  and  $d_{yz}$  symmetry) overlap with the adjacent Ce layer where

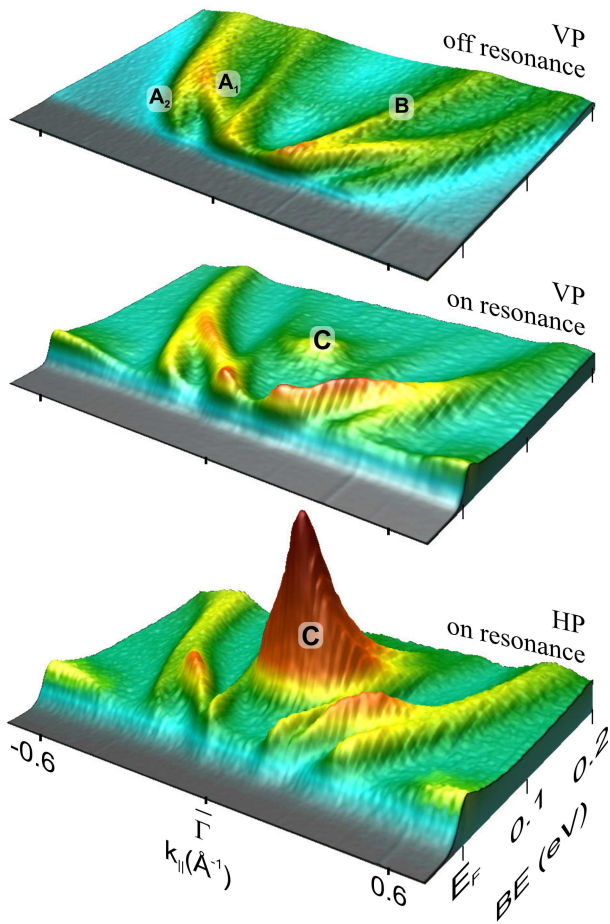


FIG. 2: (Color online) ARPES images taken along the  $\bar{\Gamma} - \bar{M}$  direction with the VP light at  $h\nu=112$  eV (top, off resonance for  $f$  emission), 121 eV (middle, on resonance for  $f$  emission), and with the HP light at  $h\nu=121$  eV (bottom, sensitive to the  $d_{3z^2-r^2}$  orbitals).

they exhibit linear combinations of  $f$  symmetry at the Ce sites, and are thus allowed for hybridization with the Ce  $4f$  states. The experimentally observed behavior of band  $A_1$  may reflect effects of such hybridization, since it strongly deviates from a parabolic dispersion. In order to get a rough estimate of this effect, results of calculations, where the  $4f$  states are treated as valence band states, are shown in Fig. 1(d). Due to their interaction with the  $f$  states, Fe  $d_{3z^2-r^2}$  do not contribute anymore to the band structure close to  $E_F$ . Instead, a band of this symmetry appears at about 0.33 eV BE at the  $\bar{\Gamma}$  point.

An investigation of the discussed hybridization between the Fe  $3d_{3z^2-r^2}$ -derived bands and the Ce  $4f$  states is possible enhancing the cross section of photoexcitation by switching from VP to HP ( $3d$  bands) and exploiting the  $4d \rightarrow 4f$  Fano resonance ( $4f$  states). Respective PE maps are shown in Fig. 2. In the topmost map, taken with VP at  $h\nu=112$  eV bands  $A_1$ ,  $A_2$  and  $B$  are of comparable intensity, reflecting their Fe  $3d_{xz,yz}$  and  $3d_{x^2-y^2}$  character. Switching to  $h\nu=121$  eV

the intensity of bands  $A_1$  and  $A_2$  becomes essentially larger as compared to that of band  $B$ . This is caused by resonant enhancement of partial  $4f$  admixtures to the former bands. Especially the intensity of band  $A_1$  grows strongly between 0.1 eV BE and the Fermi level, supporting the former assumption about the hybridization with Ce  $4f$  states. In addition two other features appear: (i) a peak directly at  $E_F$  that reflects the Ce  $4f^1$  final state and (ii) a further band with its top at about 0.1 eV BE, labeled  $C$ . Finally, at HP and  $h\nu=121$  eV (Fig. 2 bottom), band  $C$  appears extremely enhanced, indicating its predominant  $3d_{3z^2-r^2}$  character. Thus, its visibility at 121 eV and VP is only due to finite Ce  $4f$  admixtures. Band  $A_3$ , on the other hand, is still not observed.

In the results of our calculations [see Fig. 1(d)] the Fe  $3d_{3z^2-r^2}$ -derived band at 0.33 eV BE corresponds to band  $C$ , but the calculated band has higher BE as compared to the experiment due to well known overestimation of the  $4f$ -VB interaction obtained with LDA. In Fig. 1(c) this band is absent (the respective subsurface Fe  $3d$  states form band  $A_3$ ), however, a similar band [small dots in Fig. 1(c)] is found at 0.25 eV BE which is derived from the Fe  $3d$  states of the central (bulk) layer. Thus, a possible presence of Ce at the surface may influence band  $C$  and other bands of  $3d_{3z^2-r^2}$  character.

In order to investigate this effect, the calculations were repeated for a Ce terminated slab [see Fig. 3(a)]. The results reveal at the  $\bar{\Gamma}$  point the formation of a surface-derived band of  $3d_{3z^2-r^2}$  symmetry close to the experimentally obtained position of band  $C$ , while band  $A_3$  is not observed. The remaining band structure looks quite similar to the one calculated for the P terminated slab.

One can see in Fig. 1(d), that the lowest lying Ce  $4f$ -derived band is pushed above  $E_F$  in that regions of  $\mathbf{k}$  space, where it interacts with the valence bands. This is in interesting correspondence to the experimentally observed behavior of the  $4f^1$ -derived feature at  $E_F$  [Fig. 2, on resonance]: Around the  $\bar{\Gamma}$  point this feature disappears and seems to be pushed across the Fermi energy by the parabolic valence bands, that in turn reveal certain  $4f$  admixtures in this region of  $\mathbf{k}$  space. Similar interaction phenomena have been reported for the Yb  $4f^{13}$  bulk emission of the heavy-fermion system YbRh<sub>2</sub>Si<sub>2</sub> [18] as well as for the respective surface component of YbIr<sub>2</sub>Si<sub>2</sub> [20, 21]. In the latter case, where the  $4f$  emission is relatively far away from the Fermi energy (0.6 eV BE), the phenomenon could be described quantitatively in the light of a simplified approach to the Periodic Anderson Model (PAM) where  $4f$  dispersion and  $4f$  admixtures to the valence bands are explained by linear combinations of  $4f$  and valence-band states. For  $4f$  emissions at  $E_F$  the mentioned approach is, unfortunately, not applicable because interaction with unoccupied valence states is not properly considered. In order to solve this problem we present in the following an elaborated approach to PAM based on dynamical mean-field theory (DMFT).

For a numerical simulation of hybridization effects within PAM we consider a valence band of bandwidth  $W=1.2$  eV and center at  $\epsilon_d=0.7$  eV BE, with parabolic dispersion in the relevant part of  $\mathbf{k}$  space and a  $4f$  state at  $\epsilon_f=2$  eV BE. The

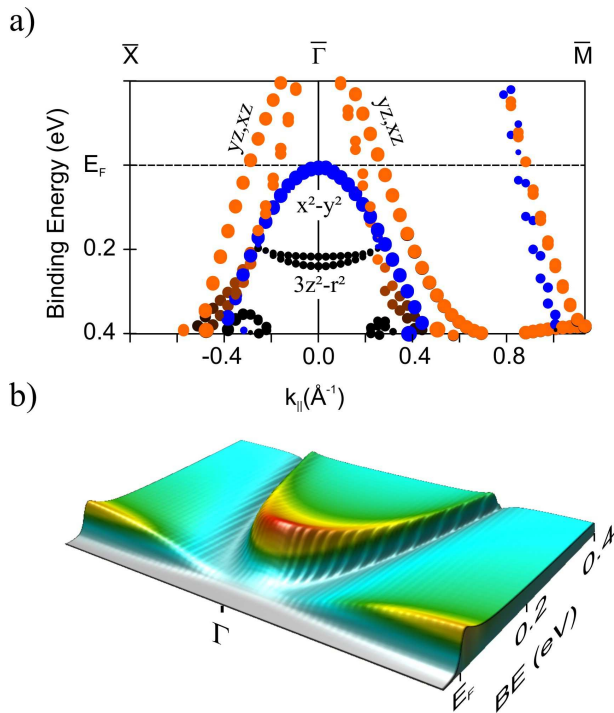


FIG. 3: (Color online) (a) Calculated energy bands for a Ce terminated slab constructed by interchanging the FeP and CeO stacks of the slab shown in Fig. 1(c). The meaning of the symbols is the same as in Fig. 1(c) and (d). (b) Distribution of the spectral intensity calculated by means of the Periodic Anderson Model.

self-energy was calculated by DMFT in a way as recently proposed in Ref. [22] but applying the noncrossing approximation (NCA) [23] as impurity solver like in Ref. [24]. With a hybridization parameter  $t_{df}=0.3$  eV and an on-site Coulomb repulsion  $U=7$  eV the DMFT equation provides the self-energy of the hybridized  $4f$  states. Results in Fig. 3(b) show, that the peak at  $E_F$  is caused by  $f$ - $d$  hybridization and might be interpreted as the tail of the Kondo resonance, which is located above  $E_F$  [25]. For those  $\mathbf{k}$  values where the VB comes close to the Fermi level, the  $f$  state is pushed towards lower BE (above  $E_F$ ) as reflected in the PE spectrum by a decrease of  $4f$ -derived intensity at  $E_F$ , while the intensity of the interacting valence band becomes enhanced by substantial  $4f$  admixtures.

In our study, we compared ARPES data of CeFePO with results of LDA slab calculations and analyzed the effect of  $f$ - $d$  hybridization both in the framework of LDA and PAM. Without adjustment of internal lattice parameters, our slab calculations reproduce qualitatively the observed band dispersions and characters, demonstrating the importance of surface effects in the electronic structure. Particularly the termination of the surface either by P or Ce atoms affects strongly shape and position of the bands. For an interpretation of the experimental data a coexistence of both terminations must be considered.

Strongest influence of the surface effects is found for the Fe

$3d_{3z^2-r^2}$  orbitals, which have largest overlap and, therefore, mostly pronounced interaction with the Ce-derived states. As a consequence, a missing Ce surface layer induces the formation of surface-derived bands which are not observed in bulk band structure. In LaFePO the Fe  $3d_{3z^2-r^2}$ -derived states form a pocket in the Fermi surface around the  $\bar{\Gamma}$  point, that is reproduced by our slab calculations if interactions with the  $4f$  states are neglected [Fig. 1(c)]. In CeFePO this pocket is missing due to the  $f$ - $d$  hybridization [Fig. 1(d)].

The Fe  $3d_{xz,yz}$ -derived states are not so strongly affected by the hybridization. Two bands of this symmetry cross the Fermi level near  $\bar{\Gamma}$ , while two others exhibit intersections near the  $\bar{M}$  point. In LaFePO, each pair of these bands nearly degenerate, forming Fermi pockets around the  $\bar{\Gamma}$  and  $\bar{M}$  points, respectively. The different behavior of these bands in CeFePO might be also a consequence of the  $f$ - $d$  hybridization.

Superconductivity depends crucially on electronic interactions between different FS sheets. Following the discussion in Ref. [13], it is governed by nesting between a sheet around the  $M$  point and sheets at  $\Gamma$  formed by bands of  $d_{xz,yz}$  and  $d_{xy}$  symmetry, respectively. Thus the strong modifications of the Fermi surface as induced by the Ce  $4f$  states suppress superconductivity in CeFePO, which is observed in other RFePO compounds without strong  $f$ - $d$  correlation. On the other hand, also the  $4f$  states are heavily affected by interaction with the valence bands as reflected by the observed dispersion of the Kondo resonance and may be important for the understanding of quenching of magnetism and appearance of heavy-fermion properties in CeFePO.

This work was supported by the DFG projekt VY64/1-1, and by the Science and Technology Center in Ukraine (STCU), grant 4930. The authors would like to thank S. Borisenko for support at "1<sup>3</sup>-ARPES" beam line at BESSY.

- 
- [1] Y. Kamihara et al., J. Am. Chem. Soc. **130**, 3296 (2008).
  - [2] X. H. Chen et al., Nature (London) **453**, 761 (2008).
  - [3] Z.-A. Ren et al., Europhys. Lett. **82**, 57002 (2008).
  - [4] G. F. Chen et al., Phys. Rev. Lett. **100**, 247002 (2008).
  - [5] I. I. Mazin and J. Schmalian, Physica C **469**, 614 (2009).
  - [6] Y. Kamihara et al., Phys. Rev. B **78**, 184512 (2008).
  - [7] R. E. Baumbach et al., New J. Phys. **11**, 025018 (2009).
  - [8] J. Zhao et al., Nature Mater. **7**, 953 (2008).
  - [9] A. Jesche et al., New J. Phys. **11**, 103050 (2009).
  - [10] Y. Luo et al., arXiv:0907.2691 (unpublished).
  - [11] E. M. Brüning et al., Phys. Rev. Lett. **101**, 117206 (2009).
  - [12] V. Vildosola et al., Phys. Rev. B **78**, 064518 (2008).
  - [13] K. Kuroki et al., Phys. Rev. B **79**, 224511 (2009).
  - [14] D. S. Inosov et al., Phys. Rev. B **77**, 212504 (2008).
  - [15] C. Krellner and C. Geibel, J. Crystal Growth **310**, 1875 (2008).
  - [16] S. L. Molodtsov et al., Phys. Rev. B, **78**, 142 (1997).
  - [17] D. H. Lu et al., Nature (London) **455**, 81 (2008).
  - [18] D. V. Vyalikh et al., Phys. Rev. Lett. **103**, 137601 (2009).
  - [19] O.K. Andersen, Phys. Rev. B **12**, 3060 (1975).
  - [20] S. Danzenbächer et al., Phys. Rev. Lett. **96**, 106402 (2006).
  - [21] S. Danzenbächer et al., Phys. Rev. B **75**, 045109 (2007).
  - [22] G. Sordi et al., Phys. Rev. Lett. **99**, 196403 (2007); our model

coincides with theirs but we adopted the notations:  $d \rightarrow f$ , and  $p \rightarrow d$ .

[23] N.E. Bickers, Rev. Mod. Phys. **59**, 845 (1987).

[24] P. Lombardo et al., Phys. Rev. B **74**, 085116 (2006).

[25] F. Reinert et al., Phys. Rev. Lett. **87**, 106401 (2001).